Title

Highly Responsive and Thermally Reliable Near-Infrared Organic Photodiodes Utilizing Naphthalocyanine Molecules Tuned with Axial Ligands

Journal

Advanced Optical Materials, 9(4)

ISSN

2195-1071

Authors

Leem, Dong-Seok
Lee, Kwang-Hee
Li, Ning
et al.

Publication Date

2021-02-01

DOI

10.1002/adom.202001682

Peer reviewed

ADVANCED OPTICAL MATERIALS
www.advopticalmat.de

Highly Responsive and Thermally Reliable Near-Infrared Organic Photodiodes Utilizing Naphthalocyanine Molecules Tuned with Axial Ligands

Dong-Seok Leem, Kwang-Hee Lee, Ning Li, Bum Woo Park, Taejin Choi, Takkyun Ro, Oh Kyu Kwon, Young-Nam Kwon, Tse Nga Ng, and Sunghan Kim*

Achieving high-performance near-infrared (NIR) photodiodes is in great demand for potential applications like biometrics, security, artificial vision, biomedical imaging, etc. Herein, silicon naphthalocyanine (SiNc) small molecule-based NIR photodiodes with narrowband absorption are presented. The optimized photodiode by varying the axial ligand in the SiNc molecules exhibits a high external quantum efficiency of 76.6% at 795 nm with narrow full width at half maximum of 80 nm, a very low dark current of 1.07 nA cm^{-2} at a reverse bias of −3 V, and the resultant detectivity of 5.66 × 10^{12} Jones. Further increase of the detectivity up to 10^{13} Jones is obtained by modulating the applied bias to −1 V, which is among the highest values of organic NIR detectors reported to date. The SiNc-based photodiodes are further characterized by temporal response, linear dynamic range, etc., and shown to be stable in high humidity for over a month and in a remarkably wide temperature range (−55 to 125 °C). It is highly likely that the developed SiNc-based photodiodes can be applicable to a wide variety of NIR sensor platforms.

Since the initial feasibility studies on organic photodiodes (OPDs) for image sensor applications,[1,2] tremendous research progress has been made and full-color image sensors have been demonstrated with OPDs on metal-oxide active-matrix backplanes. The imagers utilized panchromatic organic molecules with additional color filters or wavelength selective absorption layers.[3–5] In addition, other applications such as X-ray imagers, health monitoring sensors, wearable electronics, etc. have been implemented using OPDs, indicative of their great potential for next generation optoelectronic devices.[5–7]

Dr. D.-S. Leem, Dr. K.-H. Lee, B. W. Park, Dr. T. Choi, T. Ro, Dr. O. K. Kwon, Y.-N. Kwon, Dr. S. Kim
Material Research Center
Samsung Advanced Institute of Technology (SAIT)
Samsung Electronics, Co., Ltd.
130 Samsung-ro, Yeongtong-gu, Suwon-si, Gyeonggi-do 16678, Republic of Korea
E-mail: ds11.leem@samsung.com
Dr. N. Li, Prof. T. N. Ng
Department of Electrical and Computer Engineering
University of California San Diego
9500 Gilman Drive, La Jolla, CA 92093-0407, USA
The ORCID identification number(s) for the author(s) of this article can be found under https://doi.org/10.1002/adom.202001682.

DOI: 10.1002/adom.202001682

Recently, interest in OPDs is moving toward extending the detection range, that is, near-infrared (NIR), in order to support a variety of new applications like biometrics, security, artificial visions, biomedical imaging, autonomous vehicles, etc.[7–12] To realize these applications, achieving high-performance NIR OPDs is in great demand. Relative to visible absorbing molecules, NIR organic molecules pose additional challenges in device performance, that is, the efficiency loss due to the reduction of energy level offsets for exciton dissociation and the high dark current owing to the decline of barrier heights for charge blocking under reverse bias.[7,9] Nonetheless, recent efforts have led to significant boosts in the performance of NIR OPDs using either polymers[10–13] or small molecule materials.[14–19] For instance, Xiong et al. investigated solution-processed polymer NIR OPDs with PMDPP3T:$PC_{61}BM$ bulk heterojunction (BHJ), exhibiting a low dark current density (J_d) of 3.0 nA cm^{-2} at −0.2 V and a high external quantum efficiency (EQE) of 48% at 850 nm (a responsivity of 0.37 A W^{-1}) for broad sensing applications.[11] A further improvement on the device performance has been recently made by introducing a very thick active layer (≈300 nm) with a non-fullerene acceptor (PTB7-Th:CO1-4Cl), achieving a high EQE of 66% at 960 nm (0.5 A W^{-1}), a low J_d of 7 nA cm^{-2} at −2 V, and a detectivity around 10^{12} Jones.[12] On the other hand, small molecule-based OPDs have also shown promising results, particularly featuring selective response to NIR wavelengths, which are mostly based on porphyrin,[14] squaraine,[15] and phthalocyanine (Pc).[16–19] Among the molecules, Pc-based NIR photodetectors have recently revealed the outstanding device performance. For example, the OPD with NIR-selective chloroindum Pc in the active layer resulted in a high EQE of 80% at 705 nm, a low J_d of 10 nA cm^{-2}, and a detectivity over 10^{12} Jones.[17] The Pc-based NIR OPDs have been further developed by utilizing chloroaluminum Pc. Lee et al. demonstrated a high EQE of 74.6% at 730 nm (0.439 A W^{-1}), a very low J_d of 1.15 nA cm^{-2} at −2 V bias, and a high detectivity over 10^{13} Jones at 0 V bias,[19] indicative of the effectiveness of organic small molecules as potential NIR photodetector applications. However, these state-of-the-art results still have limited peak responses below 750 nm. To

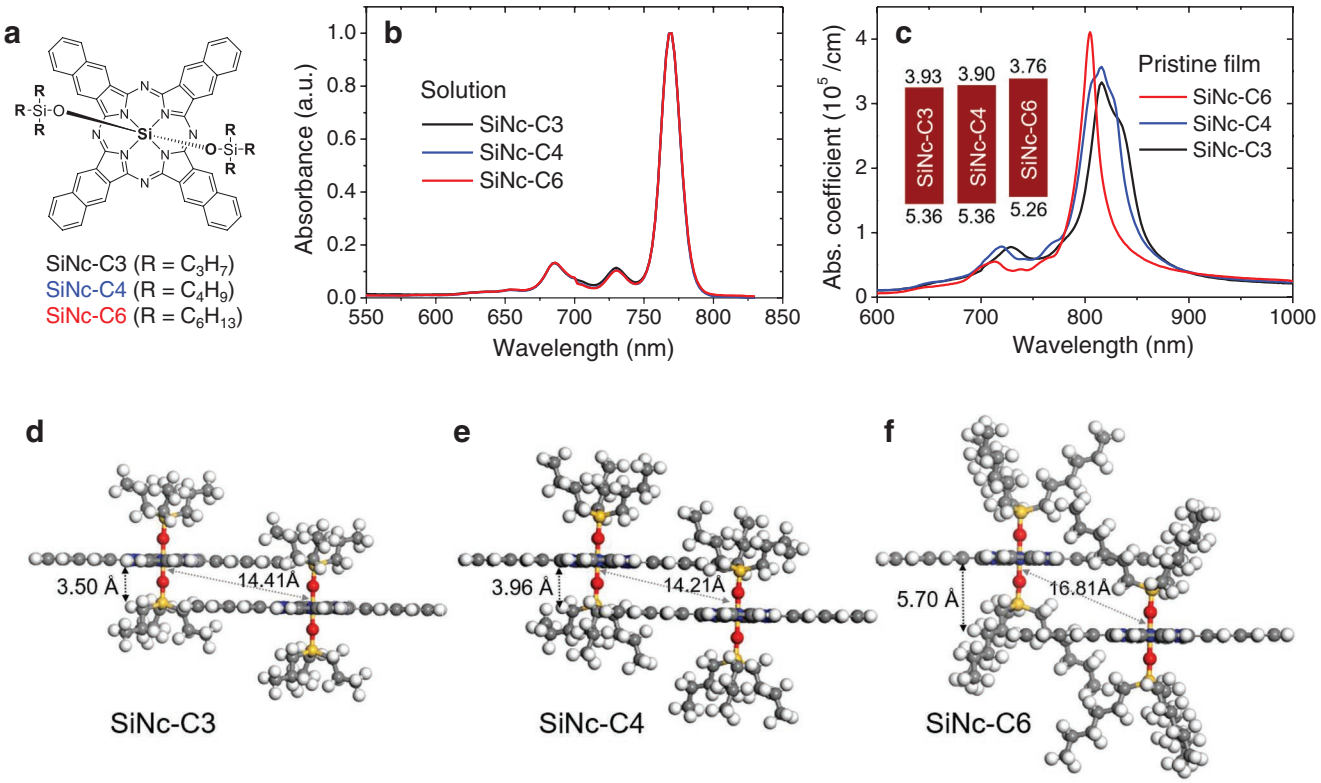

Figure 1. a) Chemical structures of the SiNc donor materials with different axial ligands. b) Normalized absorption spectra of the SiNc dissolved in dichloromethane. c) Absorption coefficient of the SiNc pristine films on glass. The inset shows energy level diagrams of the molecules. d–f) Dimer configurations of the SiNc molecules calculated by the Materials Studio package.

advance NIR OPDs to further extended wavelengths and thereby enable practical applications, further research is needed to examine NIR organic materials and device system so as to increase photo-efficiencies as well as to reach extremely low dark characteristics under bias.

Herein, we report high-performance NIR photodiodes adopting naphthalocyanine (Nc)-based small molecule as a donor material in the BHJ layer, which is known to have an extended NIR absorption compared to other Pc molecules.[20–22] Note that although Nc molecules have the advantage of the extended NIR absorption property, limited works for NIR OPDs have been made so far, exhibiting a low detectivity of 10^{10} Jones.[20] In this study, we have selected silicon naphthalocyanine (SiNc) small molecule for the NIR OPD characterization. Although the optical properties of the SiNc molecule are promising, that is, high absorption coefficient in the NIR region and very narrow full width at half maximum (FWHM),[22] a feasibility study on the fabrication of NIR OPDs has not been done. We investigated the structure-function relationship of SiNc OPDs as the axial ligands are varied; with optimization, the OPDs demonstrate detectivity up to 10^{13} Jones, which to the best of our knowledge are among the highest values[10,12,18,19] of organic NIR detectors reported to date. In addition, the devices show narrowband absorption in the NIR wavelength and transparency in the visible wavelength that will benefit integration with visible photodetectors or in augmented reality eyewear. The SiNc-based OPDs are characterized to determine metrics including temporal response, linear dynamic range (LDR), etc., and shown to be stable in high humidity for over a month and in a remarkably wide temperature range (–55 to 125 °C).

Figure 1a shows the chemical structures of SiNc molecules used as donors in this study. In particular, three different alkyl chain lengths—propyl, butyl, and hexyl—are introduced as axial ligands in order to observe the influence on the device property. The three variants are denoted as SiNc-C3, SiNc-C4, and SiNc-C6, respectively. The absorption spectra of donor solutions and their corresponding films are shown in Figure 1b,c. The energy levels of these materials are included in the inset of Figure 1c. All SiNc molecules exhibit very narrow NIR absorption profiles in dichloromethane solutions (λ = 770 nm), while the films are slightly red-shifted with widened absorption spectra depending on the axial ligands (absorption coefficients: $\geq 3.3 \times 10^5$ cm^{-1} at λ_{max} = 805–815 nm, FWHM: < 50 nm). It can be observed that at vibronic shoulder absorptions between 825 and 835 nm, the SiNc-C3 and -C4 are more red-shifted than -C6, likely due to a higher degree of intermolecular interaction between the molecules with shorter alkyl chains.[22–24] The computed dimer configurations in Figure 1d–f exhibit different intermolecular spacings of 3.50 Å (SiNc-C3), 3.96 Å (SiNc-C4), and 5.70 Å (SiNc-C6), verifying that short ligands tend to make close-packed dimers.

To evaluate material properties, OPDs were fabricated on ITO-coated glass by sequentially depositing a hole extraction layer of a triphenylaminederivative,[25] a BHJ absorbing layer comprised of SiNc and fullerene C_{60}, an electron extraction layer of C_{60}, and an ITO top electrode (see **Figure 2**a,b and

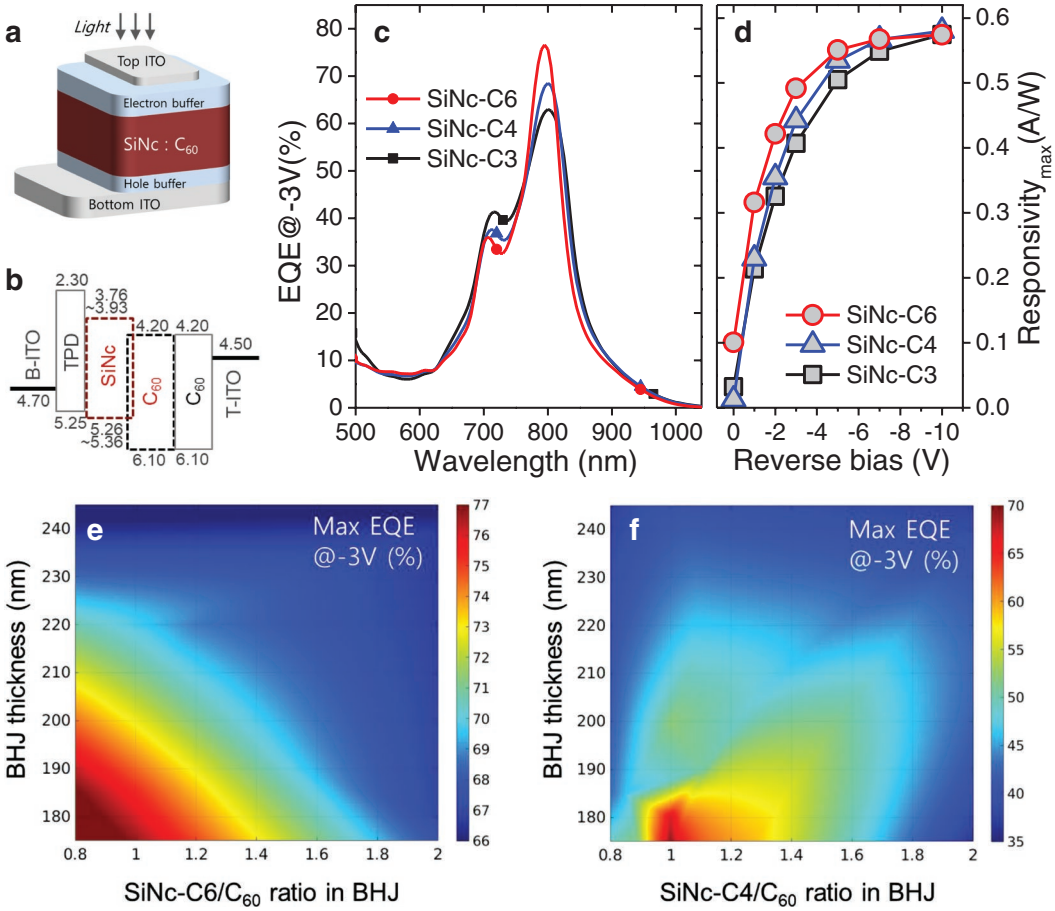

Figure 2. a) Device structure and b) energy level diagram of the SiNc OPDs. c) EQE of the OPDs measured at –3 V bias. d) Bias-dependent responsivity of OPDs. EQE contour plots of the OPDs with e) SiNc-C6 donor and f) SiNc-C4 donor in the BHJs.

Experimental Section for details). Due to high transparency of both ITO electrodes and the selective NIR absorption of the BHJ layer, OPDs are transparent to visible light (40–67% in the wavelength of 500–700 nm) as shown in Figure S1, Supporting Information.

Figure 2c shows the EQE of optimized OPDs measured at a reverse bias of –3 V bearing the SiNc donor (*p*) materials with different axial ligands and the C_{60} acceptor (*n*) in *p*/*n* ratios of 0.85–1.0 (see Table S1, Supporting Information, for the detailed blend composition). All OPDs reveal highly selective responses to NIR light with EQEs greater than 63% at wavelengths near 800 nm. Specifically, the maximum EQEs of 63% at 800 nm ($R \approx 0.41$ A W^{-1}), 68.5% at 800 nm ($R \approx 0.44$ A W^{-1}), and 76.6% at 795 nm ($R \approx 0.49$ A W^{-1}) are obtained for OPDs with SiNc-C3, -C4, and -C6 as donor materials in the BHJ blend, respectively. In particular, the SiNc-C6 device displays the narrowest FWHM of ≈80 nm, which can be beneficial for filter-free narrowband sensing applications.[6] We note that all absorption properties of OPDs are marginally blue-shifted from the peak absorption of 805–815 nm in pristine films (Figure 1c) to 795–805 nm in blend films (Figure 2c and Figure S2, Supporting Information), implying that direct interactions between donor molecules are slightly mitigated by mixing them with the C_{60} acceptor in the BHJ layer. Nonetheless, we still observed a change in the blend absorption as a function of the ligand variant of the SiNc molecule (see Figure S2, Supporting Information). This result confirms the dependence of intermolecular interactions on the axial ligand of the donor material, that is, as the intermolecular interaction weakens in the SiNc with longer alkyl chains, the blue-shift in absorption increases.

The bias-dependent spectral response curves of the OPDs are plotted in Figure 2d. The device with SiNc-C6 exhibits higher EQE values compared to the devices with SiNc-C3 and -C4 over the entire bias conditions. A maximum responsivity (*R*) of 0.57 A W^{-1} (EQE of 89%) at a reverse bias of –10 V is reached in the device with SiNc-C6. Figure 2e,f display EQE contour plots of two representative devices with SiNc-C6 and -C4, as the p/n ratio and the total thickness of the BHJ layer are varied. The efficiencies of the SiNc-C6 device have decreased by increasing the BHJ thickness due to the reduced electric field, but the peak EQEs are still maintained to be above 66% (Figure 2e) over a wide composition (see Figure S3, Supporting Information, for detailed EQE spectra). Whereas the efficiencies of the SiNc-C4 device are considerably deteriorated when either the donor-acceptor ratio changes or BHJ thickness increases, resulting in peak EQEs lower than 40% (Figure 2f).

Analysis of the internal quantum efficiency (IQE) provides insight into the dependence of device characteristics on the axial ligand of the SiNc molecules. The IQE is described by the expression EQE = $\eta_{abs} \times$ IQE.[26] The maximum device

absorption efficiency (η_{abs}) was measured to be as high as 90%, 93.1%, and 91.7% for OPDs with SiNc-C3, -C4, and -C6, respectively. Considering that there was no reflective electrode in the OPDs, the high η_{abs} (greater than 90%) are remarkable and attributed to high absorption coefficients of SiNc molecules. Based on the measured EQE and η_{abs}, the IQE was then estimated to be 70%, 73.6%, and 83.5% for the corresponding OPDs at −3 V reverse bias, with the highest IQE for the SiNc-C6 device.

Measurement of the transit time as obtained via transient photocurrent analysis[26] in Figure S4, Supporting Information, has determined the mobility to be 8×10^{-5} cm^2 V^{-1} s^{-1} for the device with SiNc-C6, and decreasing values of 6×10^{-5} and 5×10^{-5} cm^2 V^{-1} s^{-1} for OPDs with SiNc-C4 and -C3, respectively. Thus, we ascribe that superior EQE of the SiNc-C6 is mainly attributed to higher IQE (i.e., higher probability of the charge separation and collection) accompanied with the enhanced charge carrier mobility in the BHJ layer.[23,26] A similar result was reported by Zhang et al.,[23] showing that the introduction of bulky substituents in the molecular backbone weakened the π–π interaction between molecules in the BHJ layer and then suppressed the formation of large phase-separated domains (aggregation), which resulted in the enhanced charge transport property and the consequent improvement in the overall efficiency in the photodiode. We have further investigated the axial ligand effects on the charge transport of the SiNc molecule by simulating the P—N dimer configuration. The module Blends was used to predict the mixing energy and the interaction parameters (χ) based on the Flory–Huggins theory.[27,28] The calculated χ parameters were found to increase with the reduction in the chain length. For instance, the SiNc-C3, -C4, and -C6 exhibit χ values of −15.3, −23.5, and −26.0, respectively. Since the lower number indicates a more homogeneous mixing between two molecules (SiNc and C60), it is highly likely that the SiNc-C6 can form more homogeneous blend for efficient charge dissociation, whereas the SiNc-C3 with the relatively higher χ value tends to make the blend system de-mixing with phase separation (aggregation), which is unfavorable for the efficient charge transporting property.[23,28,29] On the other hand, in terms of the energy levels shown in the inset of Figures 1c and 2b, employing the hexyl ligand in the SiNc pushes the lowest unoccupied molecular orbital (LUMO) level up and thus increases the donor–acceptor LUMO offset, that is, the driving force for efficient exciton dissociation.[26]

Figure 3a presents the current density versus voltage (*J*-*V*) characteristics of the OPDs measured in the dark. The SiNc-C6 and -C4 devices exhibit remarkably low J_d values of 1.07×10^{-9} and 1.98×10^{-9} A cm^{-2} at a reverse bias of −3 V, respectively. Note that devices without buffer layers revealed an order of magnitude higher dark current as shown in Figure S5, Supporting Information. For instance, the SiNc-C6 device without buffer layers exhibits 3.65×10^{-8} A cm^{-2} at −3 V. Introducing a TPD hole buffer results in a slight reduction in the dark *J*-*V* (9.52×10^{-9} A cm^{-2} at −3 V), indicative of the effective role as the electron blocking layer. However, this value is still higher than that (1.07×10^{-9} A cm^{-2}) obtained from the optimized SiNc-C6 device with both hole (TPD) and electron (C_{60}) buffers. Therefore, low J_d values of the optimized device are attributed to both charge blocking layers inserted at the interface between the BHJ and the bottom/top electrodes[7,25] as schematically shown in Figure 2b. On the other hand, the SiNc-C3 device shows a relatively high J_d value of 2.59×10^{-8} A cm^{-2} at −3 V bias, despite that it has the same device geometry including the same active layer thickness as the others. Morphological changes are one possible parameter affecting J_d, but no significant differences were seen among the SiNc OPDs with different axial ligands in atomic force microscopy as shown in Figure S6, Supporting Information. Hence, there are additional governing parameters on the dark current such as bulk thermal generation,[7,8] trap-mediated recombination,[7] etc. that might have adversely affected the J_d in the SiNc-C3 device.

The temperature dependence of the J_d of OPDs is depicted in Figure 3b. The devices exhibit an order of magnitude increase in the J_d from 0 to 63°C, which is comparable to the visible OPDs with larger bandgaps and even superior to the conventional silicon PDs,[30] indicative of high thermal stability in dark characteristics of SiNc-based NIR OPDs used in this study. The dark current thermal activation energy (E_a) determined from the slope of the Arrhenius plots is shown in Figure S7, Supporting Information. Note that the E_a values are an additional monitoring factor to estimate the influence of bulk thermal generation.[31,32] The E_a values are quite low and very similar (0.27–0.34 eV), and still far below the optical bandgap (Figure 1c), suggesting that the bulk thermal generation is not a major contributor to the dark current within SiNc-based OPDs.

While we have measured very low J_d values in the SiNc-OPDs, it is crucial to accurately determine the total noise characteristics of OPDs.[6–8,33,34] Figure 3c exhibits the total noise currents (i_n) of OPDs measured as a function of bandwidth in relation with $i_n = [i_{shot}^2 + i_{thermal}^2 + i_{1/f}^2 + ...]^{1/2}$, where $i_{1/f}$ is the flicker noise. All OPDs show the frequency-dependent flicker noise component, but OPDs with SiNc-C6 and -C4 still show lower noise values than the SiNc-C3 device in the whole frequency range. A widely used figure of merit to represent the signal-to-noise ratio is the specific detectivity (D^*), which was calculated by

$$D^* = \frac{R\sqrt{A\,B}}{i_n} \tag{1}$$

where A is the detecting area of the device, B is the bandwidth and R is the responsivity. Note that for the calculation of D^*, the noise data measured at 45 Hz were selected, which is the same frequency used for the R measurement. The calculated D^* values of OPDs at −3 V bias are shown in Figure 3d. The devices with SiNc-C6 and -C4 have similarly high D^* of 5.66×10^{12} cm Hz$^{0.5}$ W^{-1} at 795 nm and 5.88×10^{12} cm Hz$^{0.5}$ W^{-1} at 800 nm, respectively, whereas the SiNc-C3 device show a $D^*$of 3.39×10^{12} cm Hz$^{0.5}$ W^{-1} at 800 nm due to lower R and higher noise current than the other devices. The bias-dependent noise currents of OPDs are plotted in Figure 3e. The noise currents of all devices decrease with reducing the applied reverse bias, and a minimum noise level of 2.29×10^{-14} A Hz$^{-0.5}$ at a reverse bias of −1 V was measured in the SiNc-C6 device. Since this device shows a high R of 0.32 A W^{-1} (EQE of 49.3%) at −1 V bias (see Figure 2d), it follows that the D^*value was calculated to reach 1.85×10^{13} cm Hz$^{0.5}$ W^{-1} at 795 nm as shown in Figure 3f. To the best of our knowledge, this is among the

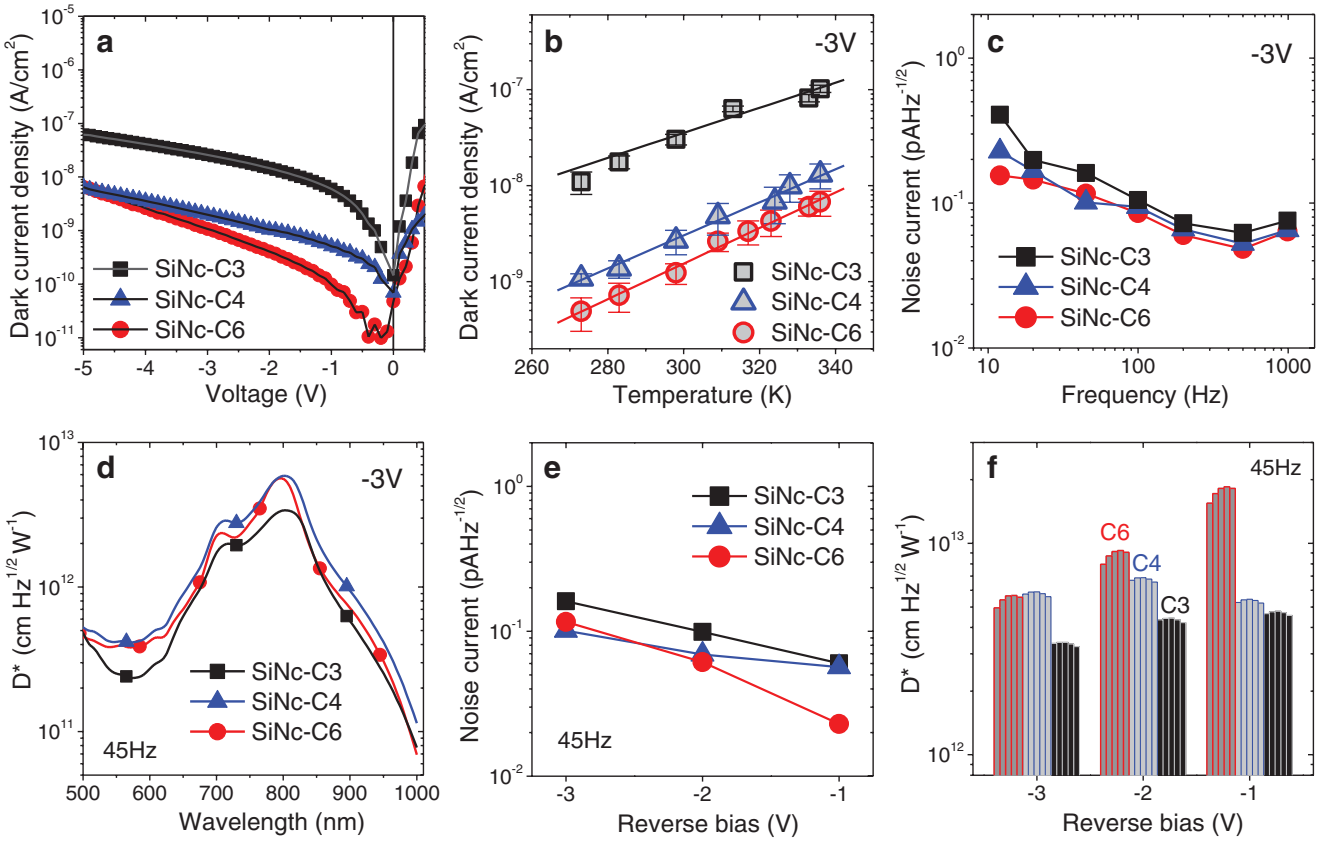

Figure 3. a) *J–V* characteristics of the OPDs in the dark. b) Temperature dependent *J–V* characteristics in the dark. c) Noise current density measured by a power spectrum analyzer. d) Specific detectivity of the OPDs. e) Plot of noise current of the OPDs versus reverse bias. f) Bias-dependent specific detectivity of the OPDs. The values are extracted from the data between 790 to 810 nm, and each bar represents an increment of 5 nm.

highest D^* values seen in NIR OPDs reported to date.[7,10,12,18,19] All measurements are further summarized in Table S1, Supporting Information.

As the response speed in a photodetector is crucial to many applications, the temporal characteristics of OPDs are examined under microsecond pulses of NIR light illumination with the intensity of 1 mW cm^{-2}, as shown in **Figure 4**a–c. The response speed of OPDs becomes faster with the longer axial ligand in the SiNc molecule, which follows the same trend as the efficiency characteristics and the mobility data in Figure 2c and Figure S4, Supporting Information. The rise time (τ_{rise}) is determined from the time interval for the photoresponse to rise from 10 to 90% of the steady-state value[35] and is plotted against the light intensity as presented in Figure 4d. It can be clearly seen that, among the three devices, the OPD with the longest alkyl chain (e.g., SiNc-C6) exhibits the shortest τ_{rise}, independent of the light intensity. On the other hand, OPDs with SiNc-C3 and -C4 exhibit variations in τ_{rise} depending on the light intensity. This result suggests that the OPD with SiNc-C6 is governed by trap-free charge carrier dynamics, while the OPDs with SiNc-C3 and -C4 are likely controlled by charge trapping dynamics.[36] Note that the frequency response measurement on the OPD with SiNc-C6 also exhibits the fastest −3 dB cut off frequency ($f_{-3\ dB}$) of 94.2 kHz, which is pronounced than the OPD with SiNc-C4 ($f_{-3\ dB}$ ≈54.8 kHz) and -C3 ($f_{-3\ dB}$ ≈13.1 kHz) as shown in Figure S8, Supporting Information.

In addition, we have examined the temporal response of OPDs with high donor concentrations in the blend system. As observed in Figure S9a, Supporting Information, it is interesting to note that the device with a high concentration of SiNc-C6 in the blend such as p/n ratio of 2 shows little change in the photoresponse characteristics compared to the reference device. For instance, the reference and the high donor concentration devices exhibit τ_{rise} of 12 and 15 µs, respectively, under the light intensity of 0.1 mW cm^{-2}, meaning that the increase of SiNc-C6 molecules in the blend system makes little difference in the charge carrier dynamics and thus the device efficiency remains almost unchanged as shown in Figure 2e. However, for the SiNc-C4 device, the reference and the high donor concentration diodes display τ_{rise} of 22 and 38 µs in Figure S9b, Supporting Information, indicative of changes in the charge carrier dynamics attributable to the traps. Accordingly, this behavior seems to evoke a loss of efficiency when the SiNc-C4 donor concentration increases in the blend as shown in Figure 2f.

While the response speed of SiNc-based OPDs becomes faster by introducing a long axial ligand (-C6) in the SiNc molecule, the τ_{rise} is still marginally slower than a conventional Si photodetector (see Figure S9a, Supporting Information). Therefore, we have further evaluated the response characteristics under the millisecond operation condition, that is the typical frame rates used in current imaging applications.[3,7] It was revealed that the SiNc-C6 device exhibits a very similar

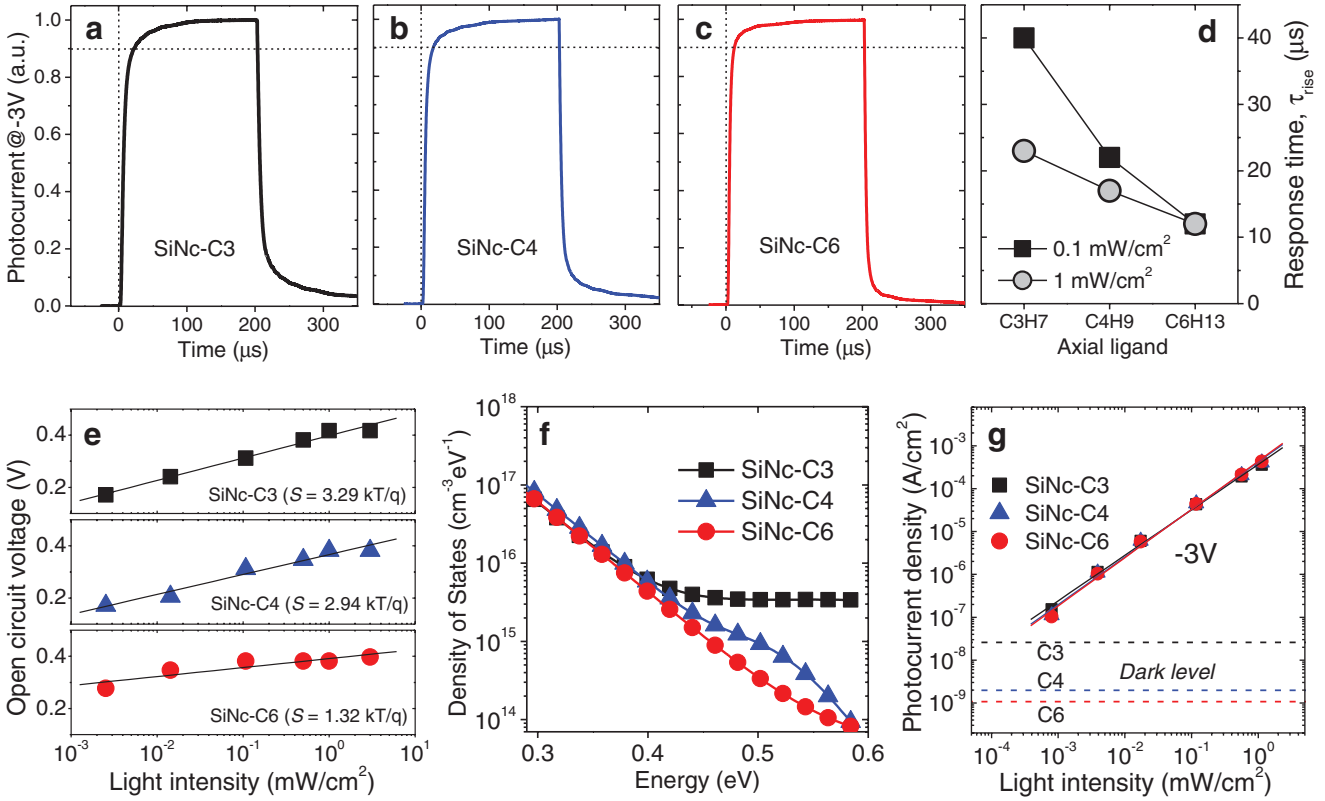

Figure 4. a–c) Photoresponse characteristics of the OPDs under illumination at 810 nm LED with the light intensity of 1 mW cm^{-2}. d) Change in the rise time of the OPDs versus the incident light intensity. e) Change of the open circuit voltage of the OPDs versus the incident light intensity. f) Density of States of the OPDs. g) Photocurrent density versus the incident light intensity.

photoresponse characteristic comparable to the Si detector when operating under 500 frames per seconds (fps) as displayed in Figure S10, Supporting Information. This indicates that our OPD is sufficiently adjustable to imaging applications utilizing the typical frame rates of 30–120 fps.

The influence of trap states on charge carrier dynamics is indicated by the logarithmic dependence of the open circuit voltage at low light intensities[37] as shown in Figure 4e. Both devices with SiNc-C3 and -C4 exhibit relatively high slopes (S) in the range of 3.29–2.94 kT q^{-1}, indicating that the trap-assisted recombination takes place in this blend system. On the other hand, the SiNc-C6 device shows a significantly reduced S value of 1.32 kT q^{-1}, which implies that the bimolecular recombination becomes dominant over trap-assisted recombination.[37] As depicted in Figure 4f, the density of states as measured by electrochemical impedance spectroscopy clearly shows the presence of deep traps in the blend systems with -C3 and -C4 axial ligands of the donor material. As such, we confirm that charge traps in the blend system of the OPD have led to the delay in the response time of OPDs and the associated decrease in the device efficiency. Moreover, we interpret that a high density of deep trap states (0.5–0.6 eV) in the SiNc-C3 may act as one plausible reason contributing to the high dark current (see Figure 3a) via trap-mediated recombination.[7,31] However, the exact mechanism needs to be further investigated.

We have evaluated the linearity of the photocurrents, namely, the LDR[25] by using LDR = 20 log J_{ph}^*/J_d, where J_{ph}^* is measured at −3 V bias under the light intensity of 1 mW cm^{-2}. As presented in Figure 4g and Figure S11, Supporting Information, the photocurrent densities of all devices increase linearly with the NIR light intensity. The SiNc-C3 device shows a LDR of 83 dB, whereas OPDs with SiNc-C4 and -C6 reveal considerably enhanced LDR values of 106 and 112 dB, respectively, attributed to the reduced J_d.

Finally, to assess the reliability of SiNc-based OPDs, we have subjected the devices to temperature-humidity tests as well as thermal shock tests. Note that the thin film encapsulation was introduced in reliability test samples, which is more practical for use in sensor integration (see Experimental Section). The representative device of SiNc-C6 (Blend p/n ratio 0.85, 220 nm) shows a remarkably high stability in 85 °C and 85% relative humidity as displayed in **Figure 5**a. It is interesting to note that the device after long-term storage shows the improved performance compared to the initial value. We speculate that this behavior is mainly associated with the thermal annealing effect on the device at 85 °C. The devices were periodically taken out of the humidity-temperature chamber and measured in ambient in order to monitor the change of the device performance. Thus, the repeated heating and cooling procedures may cause the post-annealing effect on the sample during the stability monitoring for 1000 h. Also shown in Figure 5b, the SiNc-C6 OPD (Blend p/n ratio 0.85, 200 nm) maintains the same device performance under harsh conditions like repeated cycling between −55 and 125 °C, showing that SiNc-based

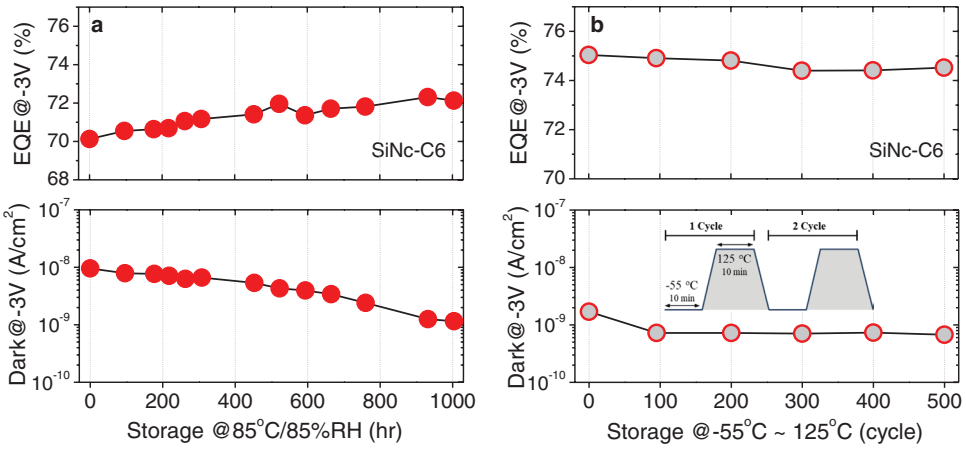

Figure 5. Stability tests of the SiNc-C6 OPD subjected to a) 85 °C/85% RH environment and b) cycling between −55 and 125 °C. Each cycle places the device at −55 °C for 10 min and 125 °C for 10 min.

photodiodes are thermally and environmentally stable with standard encapsulation.

In conclusion, we have demonstrated high-performance organic NIR photodiodes comprising SiNc small molecules with three different axial ligands. The optimized photodiode possessing the SiNc molecule with a relatively long axial ligand (SiNc-C6) has revealed a state-of-the-art EQE of 76.6% at 795 nm and a very low J_d of 1.07 nA cm^{-2} at a reverse bias of −3 V. The device performance has slightly decreased with reduced alkyl chain lengths in the SiNc molecule, mainly attributable to the loss of IQE as well as the charge carrier mobility from trap states. Additional noise measurements and the estimation of the device detectivity showed a high D^* value of 5.66×10^{12} cm Hz$^{0.5}$ W^{-1} under a reverse bias of −3 V. Further increase of D^* to 1.85×10^{13} cm Hz$^{0.5}$ W^{-1} is obtained by decreasing the applied bias to −1 V, owing to the reduced noise current, albeit at the slight expense of the responsivity (R of 0.32 A W^{-1}, EQE of 49.3%). Further analyses on the photoresponse speed and the reliability tests have proven competitive performance compared to the silicon detector, and the OPDs offer an additional advantage that they are transparent in the visible spectrum. It is highly likely that the developed SiNc-based OPDs can be applicable to a wide variety of NIR sensor platforms and facilitate novel applications.

Experimental Section

Materials and Devices Fabrication: Silicon 2,3-naphthalocyanine bis(tripropylsilyloxide) and bis(tributylsilyloxide) were synthesized according to the literature[22] followed by sublimation. Silicon 2,3-naphthalocyanine bis(trihexylsilyloxide) was purchased from Sigma–Aldrich. The OPDs were fabricated on ITO coated glass substrate by sequentially depositing a 5 nm thick triphenylamine derivative as a hole extraction layer, a BHJ absorption layer consisting of SiNc and fullerene C_{60}, and a 30 nm thick C_{60} as an electron extraction layer. The ITO top-electrode (≈10 nm, sheet resistance of 160–165 Ohm sq^{-1}) was deposited using a customized facing target RF sputtering system at a working pressure of 3 mTorr and a deposition rate of 0.06–0.07 nm s^{-1}. A 50 nm thick atomic-layer-deposited AlO_x layer was introduced on top of the OPD as an anti-reflection coating and then the device was finally encapsulated with glass cover. For the reliability test, the thin film encapsulation consisting of a 100 nm thick AlO_x layer and a 270 nm thick SiON layer was applied to the device instead of the glass encapsulation. All organic layers were thermally evaporated at 10^{-7} Torr. The pixel size, defined by the overlap of the two electrodes, was 0.04 cm^2.

Characterization and Measurements: Dimer configurations of SiNc molecules were calculated by using the module Polymorph in the Materials Studio package. The absorption spectra of the organic solutions and films were measured by a UV–VIS–NIR spectrophotometer (Shimadzu, UV-3600). The HOMO level of the organic film was measured with an AC-3 photoelectron spectrophotometer (Riken Keiki) and the LUMO level was then determined by means of the optical band gap obtained from the edge of the absorption spectrum. The current density-voltage characteristics of the devices were measured by a Keithley K4200 parameter analyzer. The photocurrent characteristics for the LDR were evaluated under illumination by a NIR LED (λ = 810 nm) with different light intensities in the range of 0.0008 – 1.0 mW cm^{-2}. The EQE was measured using a setup illuminated by monochromatic light generated by an ozone-free Xenon lamp with a chopper frequency of 45 Hz. The monochromatic light intensity was calibrated using a silicon photodiode (Hamamatsu, S1337). The photodiode noise spectral density was recorded by a power spectrum analyzer (N9020A) connected to the device through a preamplifier (SRS 570). For transient photocurrent measurements, a 520 nm pulsed laser with < 90 ns pulse width was used as the light source. The intensity of the pulsed laser was < 20 mW cm^{-2} to avoid space-charge effects. Two 1.5 V batteries connected in series with a potentiometer were used to apply a variable external bias on the photodiode. The applied voltage on the device was 2 V. The current from the biased device was transferred to voltage with a load resistor of 400 Ω and passed into the preamplifier and then recorded by an oscilloscope. Electrochemical impedance spectroscopy was measured with a potentiostat (Bio-Logic SP200) in the dark in the frequency range 2 Hz–2 MHz. The frequency response was evaluated using the measurement setup consisting of a 500-MHz bandwidth oscilloscope (LeCroy Wavejet 352A), a function generator (LeCroy WaveStation 2012), and a green laser diode (λ = 553 nm, 1 mW cm^{-2}).

Supporting Information

Supporting Information is available from the Wiley Online Library or from the author.

Conflict of Interest

The authors declare no conflict of interest.

Keywords

high detectivity, low dark current, naphthalocyanine, near-IR sensors, organic photodetectors

Received: October 22, 2020
Revised: November 23, 2020
Published online: December 4, 2020

[1] G. Yu, J. Wang, J. McElvain, A. J. Heeger, *Adv. Mater.* **1998**, *10*, 1431.
[2] T. N. Ng, W. S. Wong, M. L. Chabinyc, S. Sambandan, R. A. Street, *Appl. Phys. Lett.* **2008**, *92*, 213303.
[3] S.-J. Lim, D.-S. Leem, K.-B. Park, K.-S. Kim, S. Sul, K. Na, G. H. Lee, C.-J. Heo, K.-H. Lee, X. Bulliard, R.-I. Satoh, T. Yagi, T. Ro, D. Im, J. Jung, M. Lee, T.-Y. Lee, M. G. Han, Y. W. Jin, S. Lee, *Sci. Rep.* **2015**, *5*, 7708.
[4] K. Nishimura, S. Shishido, Y. Miyake, M. Yanagida, Y. Satou, M. Shouho, H. Kanehara, R. Sakaida, Y. Sato, J. Hirase, Y. Tomekawa, Y. Abe, H. Fujinaka, Y. Matsunaga, M. Murakami, M. Harada, Y. Inoue, *ISSCC Dig. Tech. Papers* **2018**, 82.
[5] R. D. J. Vuuren, A. Armin, A. K. Pandey, P. L. Burn, P. Meredith, *Adv. Mater.* **2016**, *28*, 4766.
[6] P. C. Y. Chow, T. Someya, *Adv. Mater.* **2020**, *32*, 1902045.
[7] G. Simone, M. J. Dyson, S. C. J. Meskers, R. A. J. Janssen, G. H. Gelinck, *Adv. Funct. Mater.* **2020**, *30*, 1904205.
[8] Z. Wu, N. Li, N. Eedugurala, J. D. Azoulay, D.-S. Leem, T. N. Ng, *npj Flexible Electron.* **2020**, *4*, 6.
[9] C. Wang, X. Zhang, W. Hu, *Chem. Soc. Rev.* **2020**, *49*, 653.
[10] B. Xie, Z. Chen, L. Ying, F. Huang, Y. Cao, *InfoMat* **2020**, *2*, 57.
[11] S. Xiong, J. Tong, L. Mao, Z. Li, F. Qin, F. Jiang, W. Meng, T. Liu, W. Li, Y. Zhou, *J. Mater. Chem. C* **2016**, *4*, 1414.
[12] J. Huang, J. Lee, J. Vollbrecht, V. V. Brus, A. L. Dixon, D. X. Cao, Z. Zhu, Z. Du, H. Wang, K. Cho, G. C. Bazan, T.-Q. Nguyen, *Adv. Mater.* **2020**, *32*, 1906027.
[13] G. Liu, T. Li, X. Zhan, H. Wu, Y. Cao, *ACS Appl. Mater. Interfaces* **2020**, *12*, 17769.
[14] L. Xiao, S. Chen, X. Chen, X. Peng, Y. Cao, X. Zhu, *J. Mater. Chem. C* **2018**, *6*, 3341.
[15] G. M. Somashekharappa, C. Govind, V. Pulikodan, M. Paul, M. A. G. Namboothiry, S. Das, V. Karunakaran, *J. Phys. Chem. C* **2020**, *124*, 21730.
[16] M.-S. Choi, S. Chae, H. J. Kim, J.-J. Kim, *ACS Appl. Mater. Interfaces* **2018**, *10*, 25614.
[17] C. W. Joo, J. Kim, J. Moon, K. M. Lee, J.-E. Pi, S.-Y. Kang, S.-D. Ahn, Y.-S. Park, D. S. Chung, *Org. Electron.* **2019**, *70*, 101.
[18] M. Wang, Y.-Z. Li, H.-C. Chen, C.-W. Liu, Y.-S. Chen, Y.-C. Lo, C.-S. Tsao, Y.-C. Huang, S.-W. Liu, K.-T. Wong, B. Hu, *Mater. Horiz.* **2020**, *7*, 1171.
[19] C.-C. Lee, R. Estrada, Y.-Z. Li, S. Biring, N. R. A. Amin, M.-Z. Li, S.-W. Liu, K.-T. Wong, *Adv. Opt. Mater.* **2020**, *8*, 2000519.
[20] S. M. Menke, R. Pandey, R. J. Holmes, *Appl. Phys. Lett.* **2012**, *101*, 223301.
[21] I. H. Campbell, *Appl. Phys. Lett.* **2010**, *97*, 033303.
[22] S. Hayashida, N. Hayashi, *Chem. Mater.* **1991**, *3*, 92.
[23] Z. Zhang, J. Miao, Z. Ding, B. Kan, B. Lin, X. Wan, W. Ma, Y. Chen, X. Long, C. Dou, J. Zhang, J. Liu, L. Wang, *Nat. Commun.* **2019**, *10*, 3271.
[24] H. Ziehlke, R. Fitzner, C. Koerner, R. Gresser, E. Reinold, P. Bauerle, K. Leo, M. K. Riede, *J. Phys. Chem. A* **2011**, *115*, 8437.
[25] D.-S. Leem, K.-H. Lee, K.-B. Park, S.-J. Lim, K.-S. Kim, *Appl. Phys. Lett.* **2013**, *103*, 043305.
[26] Z. Wu, W. Yao, A. E. London, J. D. Azoulay, T. N. Ng, *Adv. Funct. Mater.* **2018**, *28*, 1800391.
[27] R. L. C. Akkermans, *J. Chem. Phys.* **2008**, *128*, 244904.
[28] X. Bulliard, Y. W. Jin, G. H. Lee, S. Yun, D.-S. Leem, T. Ro, K.-B. Park, C.-J. Heo, R.-I. Satoh, T. Yagi, Y. S. Choi, S.-J. Lim, S. Lee, *J. Mater. Chem. C* **2016**, *4*, 1117.
[29] M. G. Han, K.-B. Park, X. Bulliard, G. H. Lee, S. Yun, D.-S. Leem, C.-J. Heo, T. Yagi, R. Sakurai, T. Ro, S.-J. Lim, S. Sul, K. Na, J. Ahn, Y. W. Jin, S. Lee, *ACS Appl. Mater. Interfaces* **2016**, *8*, 26143.
[30] M. Biele, C. M. Benavides, J. Hurdler, S. F. Tedde, C. J. Brabec, O. Schmidt, *Adv. Mater. Technol.* **2019**, *4*, 1800158.
[31] G. Simone, M. J. Dyson, C. H. L. Weijtens, S. C. J. Meskers, R. Coehoorn, R. A. J. Janssen, G. H. Gelinck, *Adv. Opt. Mater.* **2020**, *8*, 1901568.
[32] Z. Wu, W. Yao, A. E. London, J. D. Azoulay, T. N. Ng, *ACS Appl. Mater. Interfaces* **2017**, *9*, 1654.
[33] Y. Fang, A. Armin, P. Meredith, J. Huang, *Nat. Photonics* **2019**, *13*, 1.
[34] Y. Xia, L. E. Aguirre, X. Xu, O. Inganas, *Adv. Electron. Mater.* **2020**, *6*, 1901017.
[35] K.-H. Lee, G. H. Lee, D.-S. Leem, J. Lee, J. W. Chung, X. Bulliard, H. Choi, K.-B. Park, K.-S. Kim, Y. W. Jin, S. Lee, S. Y. Park, *J. Phys. Chem. C* **2014**, *118*, 13424.
[36] Z. Li, F. Gao, N. C. Greenham, C. R. McNeil, *Adv. Funct. Mater.* **2011**, *21*, 1419.
[37] V. Gupta, A. K. K. Kyaw, D. H. Wang, S. Chand, G. C. Bazan, A. J. Heeger, *Sci. Rep.* **2013**, *3*, 1965.